Supporting Information

The preparation of Ni/Mo-Based ternary electrocatalysts by the self-propagating initiated nitridation reaction and their application for efficient hydrogen production

Mengjie Hou,[a] Ruyue Lan,[b] Zhibiao Hu[c] and Zuofeng Chen*[a]

aShanghai Key Lab of Chemical Assessment and Sustainability, School of Chemical Science and Engineering, Tongji University, Shanghai 200092, China

bDepartment of Chemistry, College of Chemistry and Chemical Engineering, Xiamen University, Xiamen, Fujian 361005, China

cCollege of Chemistry and Materials Science, Longyan University, Longyan, Fujian 364012, China.

*Corresponding Author

E-mail Address: zfchen@tongji.edu.cn (Z.-F. C.)

Experimental Section

Chemicals.

Ammonia hydroxide (NH$_3$•H$_2$O, 28%), absolute ethanol (C$_2$H$_5$OH, ≥99.7%), silicon dioxide (SiO$_2$), hydrofluoric acid (HF, 40%w/w), ammonium molybdate tetrahydrate ((NH$_4$)$_6$Mo$_7$O$_{24}$•4H$_2$O, 99%) and nickel nitrate hexahydrate (Ni(NO$_3$)$_2$•6H$_2$O, 99%) were purchased from Macklin Chemical Regent Company. D(+)-glucose (99%) and tetraethyl orthosilicate (TEOS, 99.9%) were purchased from Aladdin Chemical Regent Company. Nafion solution (5 wt% in a mixture of lower aliphatic alcohols and water) and 20 wt% Pt/C were purchased from Sigma-Aldrich Chemical Regent Company. Deionized (DI) water was used in all experiments. All reagents used in this experiment were analytical grade and used without further purification.

Procedures

Preparation of monodisperse silica nanospheres. Monodisperse silica nanospheres were synthesized as templates by the Stöber method. The preparation of silica spheres involves the ammonia-catalyzed hydrolysis and condensation of TEOS in an aqueous ethanol solution. Briefly, 250 mL of absolute ethanol, 20 mL of DI water, and 15 mL

of 28% $NH_3 \cdot H_2O$ were mixed and stirred together for 1 h at room temperature. Subsequently, 15 mL of TEOS was added into the solution quickly. After stirring at room temperature for 6 h, the monodisperse silica nanospheres were collected by centrifugation. Finally, the white precipitate was washed with ethanol several times and air-dried at 50 °C overnight.

Preparation of honeycomb carbon (HCC). For the synthesis of HCC, typically, 0.5 g glucose was first added into 50 mL DI water in 500 mL beaker, and ultrasonically treated for 5 min. Then 1.0 g monodisperse silica nanospheres were added into the dispersion under vigorous stirring, and kept stirring at 70 °C until DI water were evaporated. The obtained SiO_2/glucose nanocomposites were collected, dried and grinded for 10 min. Then, SiO_2/glucose nanocomposites were placed in a porcelain boat carbonized under an Ar atmosphere at 900 °C for 3 h with a heating rate of 5 °C min^{-1}, which produced SiO_2/C. After etching out SiO_2 with a 10% HF solution for 24 h and being washed for several times with DI water, honeycomb carbon (HCC) was obtained.

Preparation of Mo₂N@HCC. This catalyst material was prepared by a weight ratio of HCC: $(NH_4)_6Mo_7O_{24} \cdot 4H_2O$ = 2: 1. First, 0.18 g $(NH_4)_6Mo_7O_{24} \cdot 4H_2O$ was added into

50 mL absolute ethanol in 100 mL beaker, and stirred for 2 h at room temperature. Then

0.36 g HCC was added into the dispersion under vigorous stirring. After stirring at room

temperature for 24 h, the mixture was collected by centrifugation, washed with absolute

ethanol for several times and subjected to air-drying. A porcelain boat containing the

as-obtained $(NH_4)_6Mo_7O_{24}$@HCC (covered by another porcelain boat) were placed in

a tube furnace in the 5% H_2/Ar blowing direction. After being annealed at 900 °C for 4

h with a ramp rate of 2 °C min^{-1} and being cooled down to room temperature, the

Mo_2N@HCC-900 °C catalyst was obtained. Other catalyst materials with the different

calcining temperature of 800 °C, 700 °C and 600 °C were also prepared by the same

procedure and named as Mo_2N@HCC-800°C, MoO_2/Mo_2N@HCC-700°C, and

MoO_2@HCC-600°C respectively.

Preparation of Mo_2C/MoO_2@HCC. The synthetic route of Mo_2C/MoO_2@HCC was

similar to that for Mo_2N@HCC but by a stepwise calcining procedure. The precursor

hybrids were placed on a porcelain boat in a quartz tube furnace and heated at 400 °C

for 2 h with a ramp of 5 °C min^{-1} and then at 900 °C for 4 h at a ramp of 2 °C min^{-1}.

Preparation of MoO_2@HCC-900°C. The synthetic route of MoO_2@HCC-900°C was

similar to that for Mo$_2$N@HCC, except that the 5% H$_2$/Ar was replaced by pure Ar.

Preparation of Ni/MoCat@HCC. This catalyst material was prepared by a molar ratio of Ni(NO$_3$)$_2$•6H$_2$O: (NH$_4$)$_6$Mo$_7$O$_{24}$•4H$_2$O = 10:1. First, 0.18 g (NH$_4$)$_6$Mo$_7$O$_{24}$•4H$_2$O and 0.42 g Ni(NO$_3$)$_2$•6H$_2$O were added into 50 mL absolute ethanol in 100 mL beaker and stirred for 2 h, giving a green solution. 0.09 g HCC was then added into the dispersion under vigorous stirring. After stirring at room temperature for another 24 h, the mixtures were collected by centrifugation, washed with absolute ethanol for several times and subjected to air-drying, resulting in the black powder. A porcelain boat containing the as-obtained black powder (covered by another porcelain boat) was loaded into a quartz tube furnace in the 5% H$_2$/Ar blowing direction. The precursor hybrids were calcined to 600 °C for 4 h with a ramp rate of 2 °C min^{-1}, giving Mo$_2$C/MoNi$_4$/Ni$_2$Mo$_3$N@HCC (Ni/MoCat@HCC) catalyst. Other catalyst materials with molar ratios of Ni(NO$_3$)$_2$•6H$_2$O: (NH$_4$)$_6$Mo$_7$O$_{24}$•4H$_2$O = 8:1 and 12:1 were also prepared by the same procedure and named as Ni/MoCat@HCC-L and Ni/MoCat@HCC-H, respectively.

Preparation of Ni$_2$Mo$_3$N@HCC. The synthetic route of Ni$_2$Mo$_3$N@HCC was similar

to that for Ni/MoCat@HCC, except that the calcining temperature was elevated to 800

°C.

Preparation of Mo₂C/MoNi₄@HCC. The synthetic route of $Mo_2C/MoNi_4$@HCC was

similar to that for Ni/MoCat@HCC but by a stepwise calcining procedure. The

precursor hybrids were placed on a porcelain boat in a quartz tube furnace and heated

at 400 °C for 2 h with a ramp of 5 °C min^{-1} and then at 600 °C for 4 h at a ramp of 2

°C min^{-1}.

Preparation of Ni/MoO₂@HCC. The synthetic route of Ni/MoO_2@HCC was similar

to that for Ni/MoCat@HCC, except that the 5% H_2/Ar was replaced by pure Ar.

Preparation of HCC-Free Ni/MoCat. The synthetic route of HCC-Free Ni/MoCat was

similar to that for Ni/MoCat@HCC, except that the monodisperse silica nanospheres

were replaced by commercial non-spherical silicon dioxide as sacrifice template.

Electrode preparation and Electrochemical measurements. Catalyst ink was typically

prepared by dispersing 4 mg of catalyst into 1 mL of water/ethanol mixture (v/v = 4:1)

solvent containing 80 μL of 5 wt% Nafion and sonicated for at least 30 min to form a

homogeneous ink. Then 5 μL of the catalyst ink (containing 18.5 μg of catalyst) was

pipetted onto a glassy carbon electrode (GCE, 0.07 cm^2 in area) of 3 mm in diameter

and dried at room temperature. The catalyst loading is 0.26 mg cm^{-2} in this study.

Current density was normalized to the geometrical area of the working electrode.

All electrochemical measurements were conducted using a CHI660E

electrochemical workstation (CH Instruments, China) in a typical three-electrode setup

with an electrolyte solution of 0.5 M H$_2$SO$_4$ solution at room temperature. Catalyst

samples were loaded on the GCE as the working electrode, and a graphite rod was used

as the counter electrode, and a saturated calomel electrode (SCE) was used as the

reference electrode, respectively. Before the electrochemical tests, the fresh working

electrode was cycled 50 times to stabilize the current and the linear sweep voltammetry

(LSV) measurement was conducted in a N$_2$-saturated 0.5 M H$_2$SO$_4$ (1 M KOH) solution

with a scan rate of 5 mV s^{-1}. The Tafel slope was obtained from the LSV plot using a

linear fit applied to points in the Tafel region. The durability of the catalyst was tested

in 0.5 M H$_2$SO$_4$ (or 1 M KOH) by electrolysis at a controlled potential of –0.12 V (or –

0.14 V). The electrochemically active surface areas (ECSA) of the catalysts are

compared on a relative scale using the capacitance of the electrochemical double layer

(C_{dl}) on the electrode-electrolyte interface. This comparison is validated, as ECSA is proportional to C_{dl}, which assumes that the measured current at the non-Faradaic region (i_C) is due to the charging of the double-layer capacitor. Thus, the current i_C is proportional to the scan rate v: $i_C = vC_{dl}$. To estimate the C_{dl}, the catalysts are loaded on the GCE using the procedure described above. Additionally, cyclic voltammograms (CV) were obtained around the open circuit potential (OCP, the non-Faradaic region) with sweep rates of 20, 40, 60, 80 and 100 mV s^{-1}. Long-term stability tests were carried out at 100 mV s^{-1}. Electrochemical impedance spectroscopy (EIS) measurements were carried out in the frequency range of 100 kHz – 0.1 Hz with an amplitude of 5 mV at the open-circuit voltage.

All the potentials reported in our work are expressed vs. the Reversible Hydrogen Electrode (RHE) with *iR* correction where the *R* was referred to the ohmic resistance arising from the electrolyte/contact resistance of the setup, measured prior to the experiment.

Instrumentation

Scanning electron microscopy (SEM) images, energy dispersive X-ray spectroscopy analysis (EDX) data and EDX mapping images were obtained at Hitachi S-4800 (Hitachi, Japan) equipped with a Horiba EDX system (X-max, silicon drift X-Ray detector). SEM images were obtained with an acceleration voltage of 3 kV, and EDX mapping images and EDX spectra were obtained with an acceleration voltage of 15 kV. The time for EDX mapping images is 15 min. Transmission electron microscopy (TEM) images, high resolution TEM (HRTEM) images and selected area electron diffraction (SAED) patterns were performed on a Tecnai G^2F20 S-Twin electron microscopy with an accelerating voltage of 200 kV.

Powder X-ray diffraction (XRD) patterns were measured by Bruker D8 Foucs equipped with ceramic monochromatized Cu Kα radiation (1.54178 Å). The corresponding working voltage and current is 40 kV and 40 mA, respectively. The scanning rate was 5º per min in 2θ and the scanning range was from 10°- 80°.

X-ray photoelectron spectroscopy (XPS) for elemental analysis was conducted on a Kratos Axis Ultra DLD X-ray Photoelectron Spectrometer using 60 W monochromated Mg Kα radiation as the X-ray source for excitation. The 500 μm X-ray spot was used

for XPS analysis. The base pressure in the analysis chamber was about 3×10^{-10} mbar. The C 1s peak (284.8 eV) was used for internal calibration. The peak resolution and fitting were processed by XPS Peak 4.1 software.

Brunauer-Emmett-Teller (BET) specific surface areas were measured by N_2 adsorption at 77 K using a volumetric unit (Micrometritics ASAP 2020). The samples loaded in a pre-weighted BET sample tube were degassed for 3 h at 200 °C prior to measurements. The pore size distribution was analyzed by the Barrett-Joyner-Halenda (BJH) method.

Dynamic Light Scattering (DLS) measurements of SiO_2 ball was carried out on a standard laser light scattering spectrometer (BI-200SM) equipped with a BI-9000 at digital time correlator (Brookhaven Instruments, Inc.) and a Mini-L30 diode laser (35 mW, 659 nm) as the light source was used.

Thermogravimetric analysis (TGA) measurements of $(NH_4)_6Mo_7O_{24} \cdot 4H_2O$ was carried out on a TGA Q500 at temperatures from 20 to 450 °C with a ramping rate of 10 °C min^{-1} under the high-purity nitrogen atmosphere.

Inductively Coupled Plasma Optical Emission Spectrometry (ICP-OES, Agilent
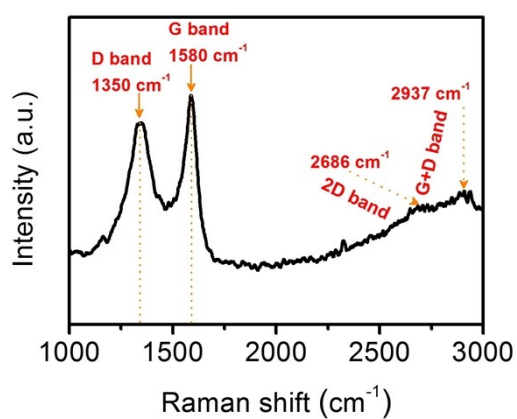
Technologies 700 Series) was used to measure the contents of Ni and Mo in the

samples. Elemental analysis (Elementar Analysensysteme GmbH) was carried out to

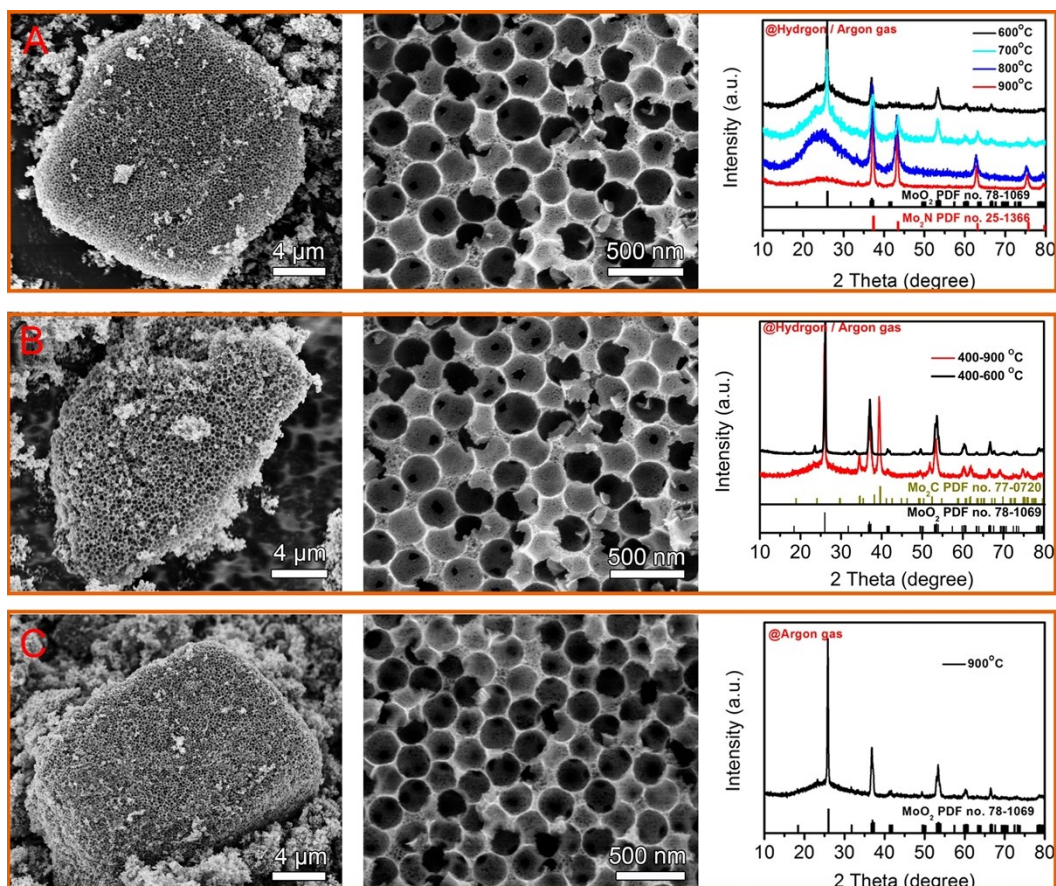measure the contents of C, N, and O in the samples.
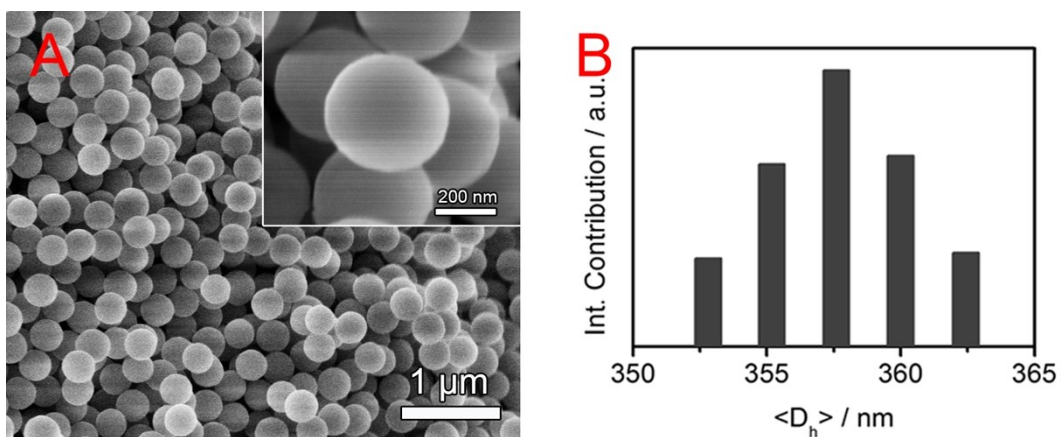
**Figure S1.** (A) SEM images and (B) DLS size distribution of the SiO$_2$ nanospheres.
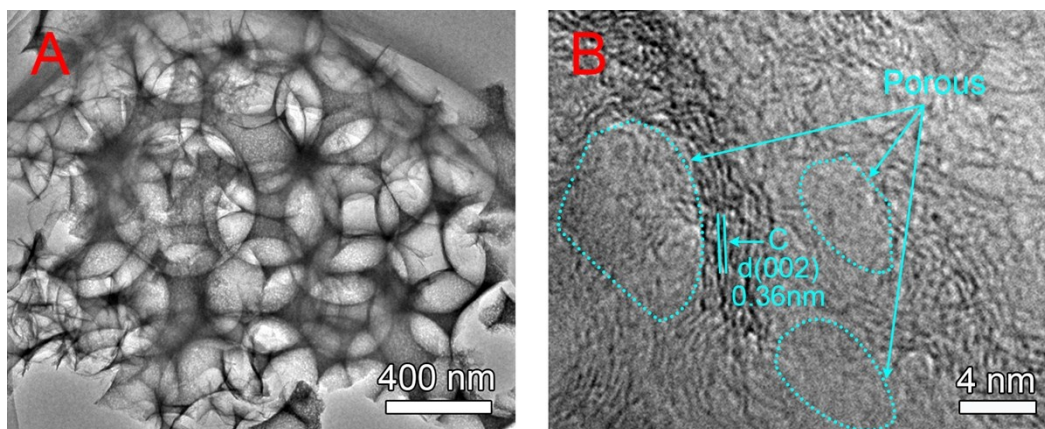
Figure S2. (A) TEM image and (B) HRTEM image of HCC.

Figure S3. Raman spectrum of HCC.

Figure S4. SEM images and XRD patterns of material samples by calcining at different temperatures for producing $Mo_2N@HCC$ (A), by a two-step calcination for producing $Mo_2C/MoO_2@HCC$ (B), and by calcining in Ar atmosphere for producing $MoO_2@HCC$ (C).
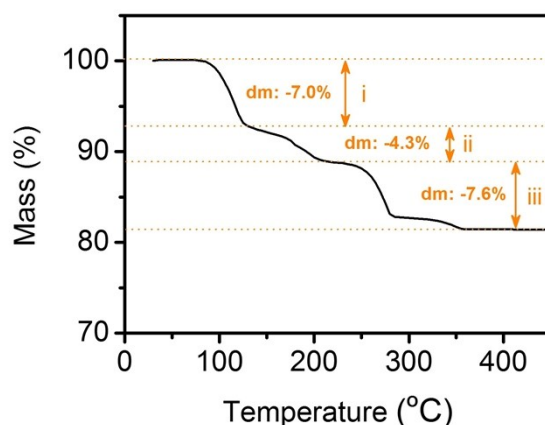
Figure S5. TG analysis of $(NH_4)_6Mo_7O_{24} \cdot 4H_2O$ under N_2 atmosphere at 10 °C/min.

As shown in Figure S5, the calculated mass loss due to the decomposition of

$(NH_4)_6Mo_7O_{24} \cdot 4H_2O$ is in accordance with the observed mass loss.

$(NH_4)_4Mo_7O_{23} \cdot 2H_2O$, $(NH_4)_2Mo_7O_{22} \cdot 2H_2O$ and MoO_3 are formed at temperature < 400

°C with the mass loss of 7.0%, 4.3% and 7.6%, respectively, at the three decomposition

steps with the release of NH_3 and H_2O. The thermal decomposition process can be

shown as follows:

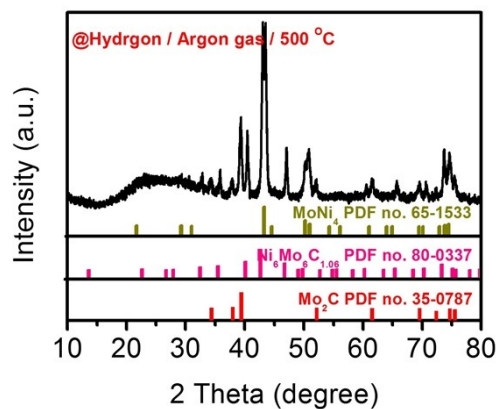Step (i). $(NH_4)_6Mo_7O_{24} \cdot 4H_2O \rightarrow (NH_4)_4Mo_7O_{23} \cdot 2H_2O + 2NH_3 + 3H_2O$ (calculated

mass loss, 7.1%.)

Step (ii). $(NH_4)_4Mo_7O_{23} \cdot 2H_2O \rightarrow (NH_4)_2Mo_7O_{22} \cdot 2H_2O + 2NH_3 + H_2O$ (calculated mass

loss, 4.4%.)

Step (iii). $(NH_4)_2Mo_7O_{22}\cdot2H_2O \rightarrow 7MoO_3 + 2NH_3 + 3H_2O$ (calculated mass loss, 7.7%.)
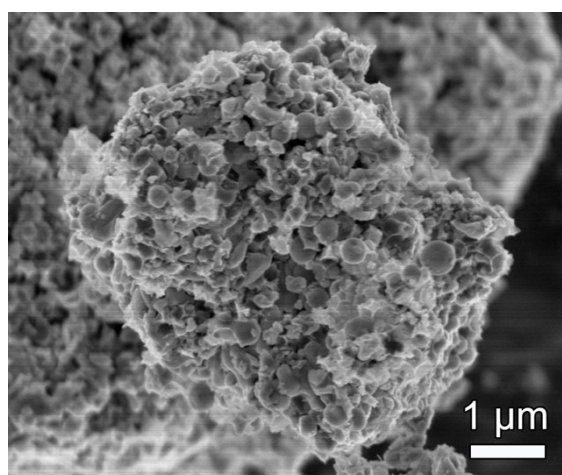

Figure S6. XRD pattern of the material prepared by calcining at 500 °C in 5% H_2/Ar atmosphere.
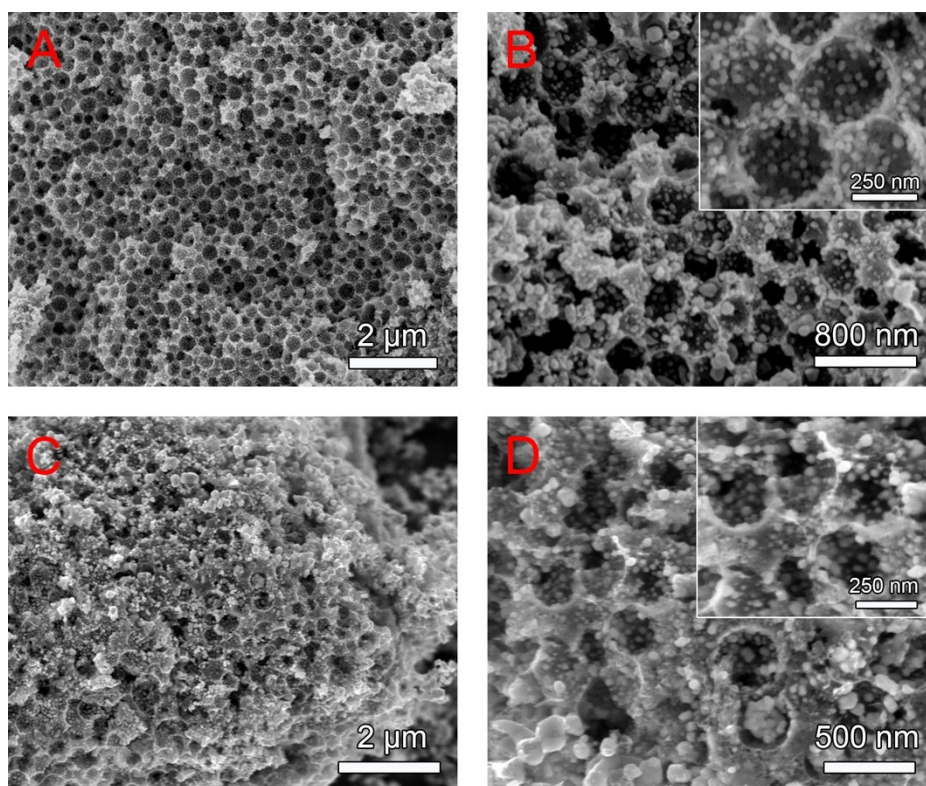
Figure S7. SEM images of (A, B) Ni/MoCat@HCC-L and (C, D) Ni/MoCat@HCC-H.
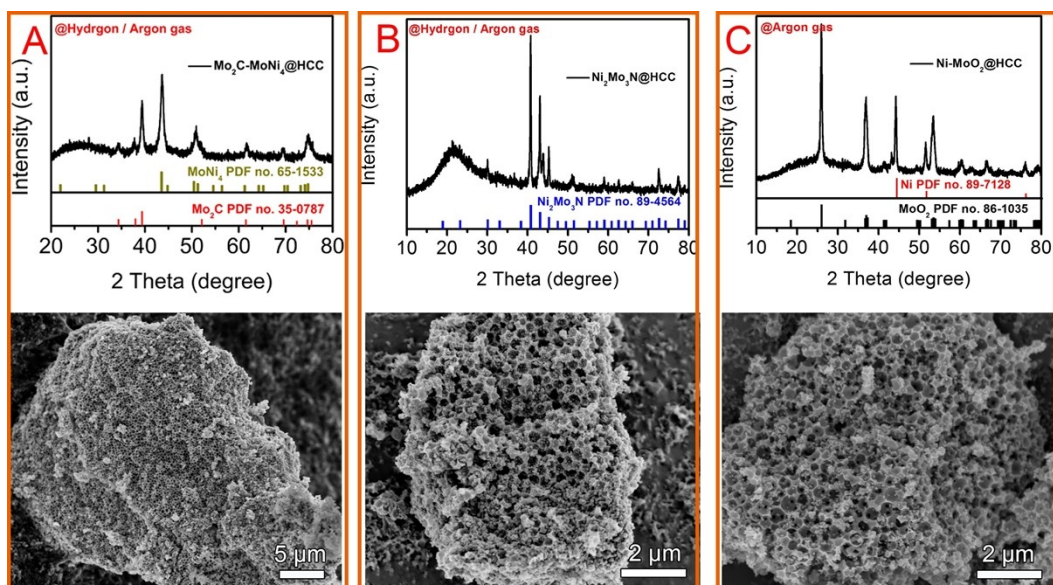
Figure S8. SEM images and XRD patterns of (A) $Mo_2C/MoNi_4$@HCC, (B) Ni_2Mo_3N@HCC, and (C) Ni/MoO_2@HCC. Note the experimental section in SI and Table 1 in the manuscript for the preparation of these contrast material catalysts.
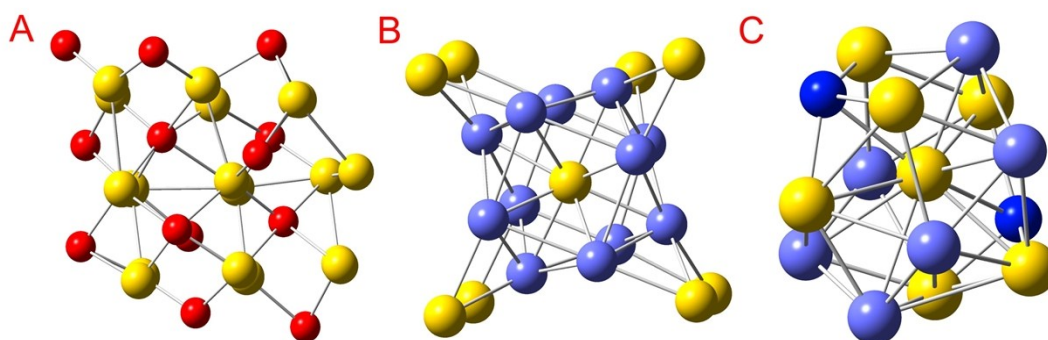

Figure S9. SEM image of HCC-Free Ni/MoCat@HCC.
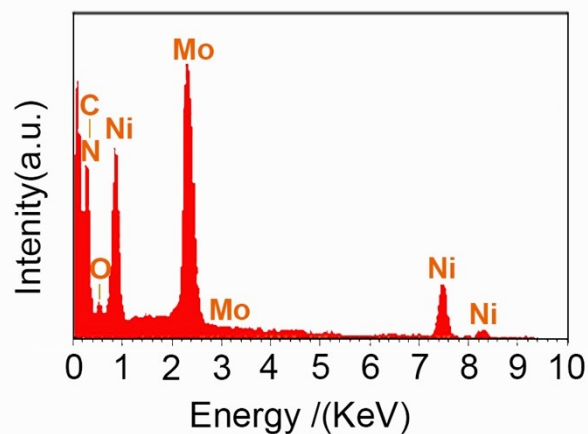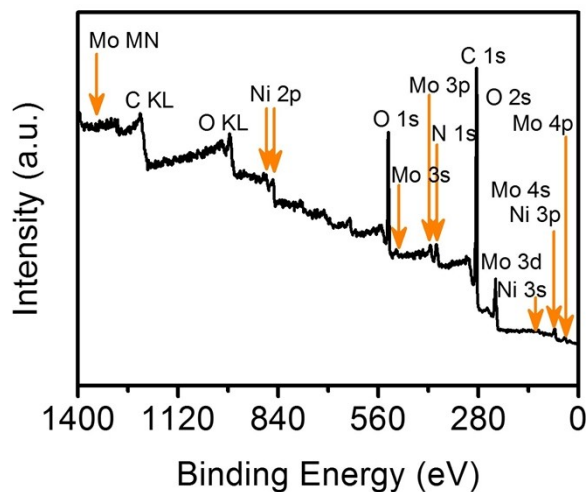
Figure S10. EDX spectrum of Ni/MoCat@HCC.

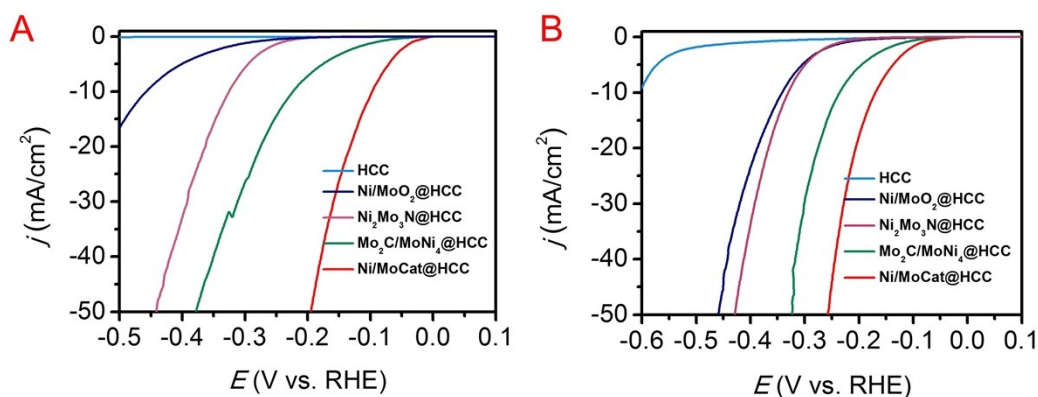**Figure S11.** Schematic representations of unit structure of (A) Mo_2C, (B) $MoNi_4$, and

(C) Ni_2Mo_3N. Note: Mo-Mo bonds only exist in Mo_2C and Ni_2Mo_3N units. Yellow

balls: Mo, purple balls: Ni, blue balls: N, and small red balls: C.

Figure S12. XPS survey spectrum of Ni/MoCat@HCC.

Figure S13. Polarization curves of Ni/MoCat@HCC, Mo$_2$C/MoNi$_4$@HCC, Ni$_2$Mo$_3$N@HCC, Ni/MoO$_2$@HCC, and HCC in 0.5 M H$_2$SO$_4$ (A) and 1 M KOH (B).

The poor performance of Ni/MoO$_2$@HCC indicates that the oxide on the surface is not an active component to the HER. The improved HER activity of Ni/MoCat@HCC (including Mo$_2$C, MoNi$_4$, and Ni$_2$Mo$_3$N) compared to Mo$_2$C/MoNi$_4$@HCC and Ni$_2$Mo$_3$N@HCC implies that the combination of three active components leads to the

best catalysis performance due to the strong electronic interaction and synergistic effect. It is also worth to note that the performance of $Mo_2C/MoNi_4@HCC$ are superior to $Ni_2Mo_3N@HCC$ in both acidic and alkaline media. Therefore, the $Mo_2C/MoNi_4$ should be the main active components for excellent HER performance of $Ni/MoCat@HCC$, and Ni_2Mo_3N is also an essential phase.
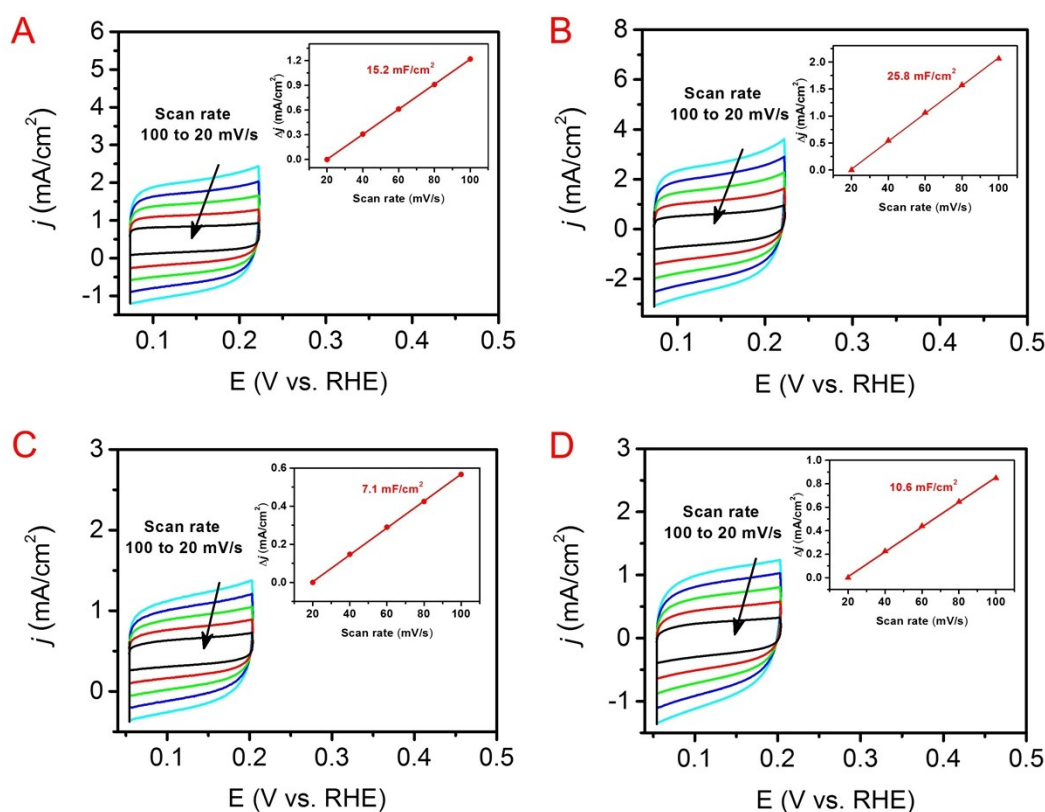
Figure S14. CV curves of Ni/MoCat@HCC-L and Ni/MoCat@HCC-H in 0.5 M H_2SO_4 solution (A, B) and in 1 M KOH solution (C, D) under different scan rates from 20 to 100 mV s^{-1}; the inset illustrates the plot of the capacitive current at 0.15 V against the scan rate.
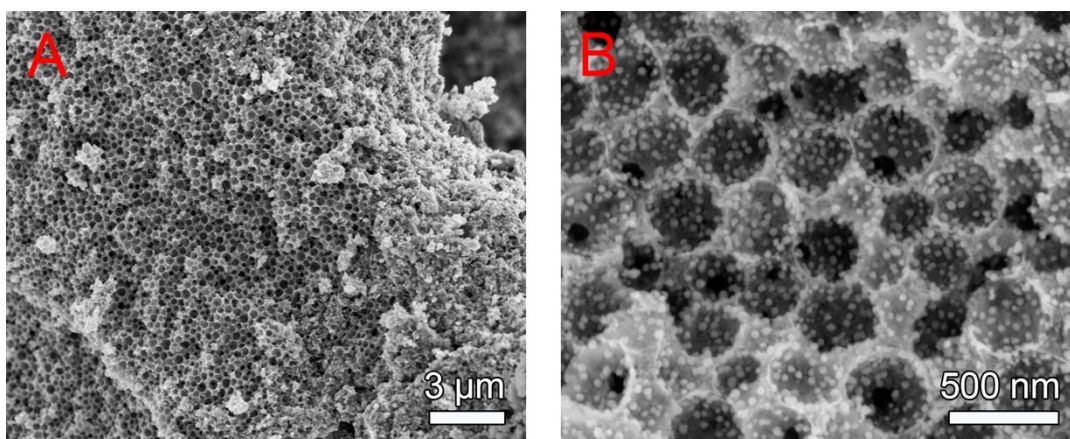
Figure S15. (A, B) SEM images of the Ni/MoCat@HCC after long-term stability test.

Table S1. Elemental analysis and ICP-OES results of Ni/MoCat@HCC.

Catalyst	C/at.%	N/at.%	O/at.%	Ni/at.%	Mo/at.%
Ni/MoCat@HCC	67.03	2.57	14.39	9.67	6.35

Table S2. Comparison of HER performance of Ni/MoCat@HCC with other Mo-based

HER electrocatalysts in 0.5 M H_2SO_4 solution.

Catalyst	j_0 (mA cm^{-2})	η_{10} (mV)	Tafel slope (mVdec^{-1})	Loading (mg cm^{-2})	Refs.
Mo$_6$Ni$_6$C	/	51	35.7	18	1
NiMoNPs/3DNG	/	56	49	0.28	2
Mo$_{0.5}$W$_{0.5}$S$_2$	0.116	138	55	0.2	3
FLNPC@MoP-NC/MoP-C/CC	0.518	74	50	2.42	4
N@MoPC$_x$-800	0.3424	108	69.4	0.14	5
MoP@HCC	/	129	48	0.26	6

MoP$_2$ NS/CC	0.83	58	63.6	7.8	7
MoP$_2$ NPs/Mo	0.06	143	57	0.18	8
MoS$_2$	0.036	167	70	1	9
N,P-doped Mo$_2$C@C	0.029	141	56	0.9	10
Mo/ Mo$_2$C-HNS	/	89	70.7	0.285	11
MoC$_x$ nano-octahedrons	0.023	142	52	0.8	12
MoO$_2$@PC-RGO	0.48	64	41	0.14	13
Mo$_2$C/CNT-GR	0.096	124	60	0.28	14
Mo$_2$C nanowires	/	130	53	0.21	15
Mo$_2$C with CNT-RGO	0.062	130	58	0.65	16
MoCN	/	145	46	0.4	17
Mo$_{0.06}$W$_{1.94}$C/CB	0.235	220	/	0.7	18
Mo$_2$C/NCF	/	144	55	0.28	19
NiMo-NGTs	0.84	65	67	2	20
Co-Mo$_2$C	/	140	39	0.14	21
Mo$_2$N-Mo$_2$C/HGr	0.062	157	55	0.337	22
MoCat	/	96	37	1.14	23
Mo$_2$C/CLCN	/	145	48.2	0.357	24
Ni/MoCat@HCC	0.099	95	74	0.26	**This work**

Table S3. Comparison of HER performance of Ni/MoCat@HCC with other Mo-based

HER electrocatalysts in 1 M KOH solution.

Catalyst	j_0 (mA cm^{-2})	η_{10} (mV)	Tafel slope (mVdec^{-1})	Loading (mg cm^{-2})	Refs.
N@MoPC$_x$-800	0.3424	108	69.4	0.14	5
MoP$_2$ NS/CC	0.83	58	63.6	7.8	7
MoP$_2$ NPs/Mo	0.06	143	57	0.18	8
N,P-doped Mo$_2$C@C	0.029	141	56	0.9	10
Mo/ Mo$_2$C-HNS	/	79	62.9	0.285	11
MoC$_x$ nano-octahedrons	0.023	142	52	0.8	12
Mo$_2$C@NC	0.096	124	60	0.28	14
Mo$_2$C/NCF	/	100	65	0.28	19
NiMoN	0.92	109	95	1.1	25
Mo$_2$N	/	353	108	0.102	26
Mo$_2$C@2D-NPCs	1.14	45	46	0.73	27
MoNi$_4$/MoO$_{3-x}$	3.42	17	36	8.7	28
Mo$_2$N-Mo$_2$C/HGr	0.479	154	68	0.337	22
Ni/ Mo$_2$C-HC800	/	123	83	0.12	29
Ni$_{2(1-x)}$Mo$_{2x}$P NWs/NF	0.537	72	/	7.4	30
Ni/MoCat@HCC	0.386	136	84	0.26	**This work**

Table S4. The exchange current density of Ni/MoCat@HCC, Ni/MoCat@HCC-L, Ni/MoCat@HCC-H and HCC-Free Ni/MoCat in both acidic and alkaline media.

Electrolyte	Ni/MoCat@HCC j_0 (mA cm^{-2})	Ni/MoCat@HCC-L j_0 (mA cm^{-2})	Ni/MoCat@HCC-H j_0 (mA cm^{-2})	HCC-Free Ni/MoCat j_0 (mA cm^{-2})
0.5 M H$_2$SO$_4$	0.099	0.052	0.065	0.038
1 M KOH	0.386	0.031	0.142	0.004

Note: The exchange current density (j_0) was calculated by the extrapolation method using the following equation: η= a + b log j, where a is the intercept on the y-axis and b is the Tafel slope. The exchange current density (j_0) is calculated when η= 0 V.

References

1. M. Y. Zu, P. F. Liu, C. Wang, Y. Wang, L. R. Zheng, B. Zhang, H. Zhao and H. G. Yang, *ACS Energy Lett.*, 2017, **3**, 78-84.

2. K. Hu, T. Ohto, L. Chen, J. Han, M. Wakisaka, Y. Nagata, J.-i. Fujita and Y. Ito, *ACS Energy Lett.*, 2018, **3**, 1539-1544.

3. H. Wang, L. Ouyang, G. Zou, C. Sun, J. Hu, X. Xiao and L. Gao, *ACS Catal.*, 2018, **8**, 9529-9536.

4. B. Liu, H. Li, B. Cao, J. Jiang, R. Gao and J. Zhang, *Adv. Funct. Mater.*, 2018, **28**, 1801527.

5. Y. Huang, J. Ge, J. Hu, J. Zhang, J. Hao and Y. Wei, *Adv. Energy Mater.*, 2018, **8**, 1701601.

6. M. Hou, X. Teng, J. Wang, Y. Liu, L. Guo, L. Ji, C. Cheng and Z. Chen, *Nanoscale*, 2018, **10**, 14594-14599.

7. W. Zhu, C. Tang, D. Liu, J. Wang, A. M. Asiri and X. Sun, *J. Mater. Chem. A*, 2016, **4**, 7169-7173.

8. Z. Pu, I. Saana Amiinu, M. Wang, Y. Yang and S. Mu, *Nanoscale*, 2016, **8**, 8500-

8504.

9. S. Du, Z. Ren, J. Zhang, J. Wu, W. Xi, J. Zhu and H. Fu, *Chem. Commun.*, 2015, **51**, 8066-8069.

10. Y.-Y. Chen, Y. Zhang, W.-J. Jiang, X. Zhang, Z. Dai, L.-J. Wan and J.-S. Hu, *ACS Nano*, 2016, **10**, 8851-8860.

11. J. Xiong, J. Li, J. Shi, X. Zhang, N.-T. Suen, Z. Liu, Y. Huang, G. Xu, W. Cai, X. Lei, L. Feng, Z. Yang, L. Huang and H. Cheng, *ACS Energy Lett.*, 2018, **3**, 341-348.

12. H. B. Wu, B. Y. Xia, L. Yu, X. Y. Yu and X. W. Lou, *Nat. Commun.*, 2015, **6**, 6512.

13. Y.-J. Tang, M.-R. Gao, C.-H. Liu, S.-L. Li, H.-L. Jiang, Y.-Q. Lan, M. Han and S.-H. Yu, *Angew. Chem. Int. Edit.*, 2015, **54**, 12928-12932.

14. Y. Liu, G. Yu, G. D. Li, Y. Sun, T. Asefa, W. Chen and X. Zou, *Angew. Chem. Int. Edit.*, 2015, **54**, 10752-10757.

15. L. Liao, S. Wang, J. Xiao, X. Bian, Y. Zhang, M. D. Scanlon, X. Hu, Y. Tang, B. Liu and H. H. Girault, *Energy Environ. Sci.*, 2014, **7**, 387-392.

16. D. H. Youn, S. Han, J. Y. Kim, J. Y. Kim, H. Park, S. H. Choi and J. S. Lee, *ACS Nano*, 2014, **8**, 5164-5173.

17. Y. Zhao, K. Kamiya, K. Hashimoto and S. Nakanishi, *J. Am. Chem. Soc.*, 2015, **137**, 110-113.

18. S. T. Hunt, T. Nimmanwudipong and Y. Román-Leshkov, *Angew. Chem. Int. Edit.*, 2014, **53**, 5131-5136.

19. Y. Huang, Q. Gong, X. Song, K. Feng, K. Nie, F. Zhao, Y. Wang, M. Zeng, J. Zhong and Y. Li, *ACS Nano*, 2016, **10**, 11337-11343.

20. T. Wang, Y. Guo, Z. Zhou, X. Chang, J. Zheng and X. Li, *ACS Nano*, 2016, **10**, 10397-10403.

21. H. Lin, N. Liu, Z. Shi, Y. Guo, Y. Tang and Q. Gao, *Adv. Funct. Mater.*, 2016, **26**, 5590-5598.

22. H. Yan, Y. Xie, Y. Jiao, A. Wu, C. Tian, X. Zhang, L. Wang and H. Fu, *Adv. Mater.*, 2018, **30**, 1704156.

23. R. Kumar, R. Rai, S. Gautam, A. De Sarkar, N. Tiwari, S. N. Jha, D. Bhattacharyya, A. K. Ganguli and V. Bagchi, *J. Mater. Chem. A*, 2017, **5**, 7764-

7768.

24. J. Jia, W. Zhou, Z. Wei, T. Xiong, G. Li, L. Zhao, X. Zhang, H. Liu, J. Zhou and S. Chen, *Nano Energy*, 2017, **41**, 749-757.

25. Y. Zhang, B. Ouyang, J. Xu, S. Chen, R. S. Rawat and H. J. Fan, *Adv. Energy Mater.*, 2016, **6**, 1600221.

26. L. Ma, L. R. L. Ting, V. Molinari, C. Giordano and B. S. Yeo, *J. Mater. Chem. A*, 2015, **3**, 8361-8368.

27. C. Lu, D. Tranca, J. Zhang, F. N. Rodri Guez Hernandez, Y. Su, X. Zhuang, F. Zhang, G. Seifert and X. Feng, *ACS Nano*, 2017, **11**, 3933-3942.

28. Y. Y. Chen, Y. Zhang, X. Zhang, T. Tang, H. Luo, S. Niu, Z. H. Dai, L. J. Wan and J. S. Hu, *Adv. Mater.*, 2017, **29**, 1703311.

29. X. Xu, F. Nosheen and X. Wang, *Chem. Mater.*, 2016, **28**, 6313-6320.

30. L. Yu, I. K. Mishra, Y. Xie, H. Zhou, J. Sun, J. Zhou, Y. Ni, D. Luo, F. Yu, Y. Yu, S. Chen and Z. Ren, *Nano Energy*, 2018, **53**, 492-500.